Electronic Supplementary Information

Homogeneous Plating/Stripping Mode with Fine Grains for Highly Reversible Zn Anode

Zhen Luo, ‡[a], Yufan Xia, ‡[a] Shuang Chen, [a] Xingxing Wu, [b] Esther Akinlabi, [c] Ben Bin Xu, *[c], Hongge Pan, [a,d] Mi Yan, [a] and Yinzhu Jiang *[a,b]

[a] School of Materials Science and Engineering, Zhejiang University, Hangzhou 310027, China

[b] Future Science Research Institute, ZJU-Hangzhou Global Scientific and Technological Innovation Center, Zhejiang University, Hangzhou 311215, China

[c] Mechanical and Construction Engineering, Faculty of Engineering and Environment, Northumbria University, Newcastle upon Tyne, NE1 8ST, United Kingdom

[d] Institute of Science and Technology for New Energy, Xi'an Technological University, Xi'an 710021, China

Corresponding authors:

E-mail address: ben.xu@northumbria.ac.uk; yzjiang@zju.edu.cn

‡ These authors contributed equally to this work.

Experimental Procedures and Calculations

1. Materials:

Zinc sulfate heptahydrate ($ZnSO_4 \cdot 7H_2O$, AR), sodium chloride (NaCl, AR), and Zn foil (99.999%) were purchased from Sinopharm Chemical Reagent Co., Ltd. Sodium sulfate (Na_2SO_4, AR) and cordycepin (Cor, 98%) were purchased from Shanghai Macklin Biochemical Technology Co., Ltd. Glass microfiber separator (GF/D) was acquired from Whatman. Ketjen black (KB) and poly(vinylidene fluoride) (PVDF) were procured from Switzerland Timcal and Sigma-Aldrich, respectively. N-methyl-2-pyrrolidone (NMP, 99.9%) and vanadium pentoxide (V_2O_5, 99.5%) were acquired from Aladdin.

2. Preparation of electrolytes

The baseline electrolyte was 2 M $ZnSO_4$ (BE). The comparison electrolytes were prepared by adding 1 mM, 5 mM, and 10 mM Cor into 2 M $ZnSO_4$ solution, denoted as BE/1Cor, BE/5Cor, and BE/10Cor, respectively. The electrolytes used in hydrogen evolution performance were 1 M Na_2SO_4 and 1 M Na_2SO_4/5 mM Cor. Ultrapure water was used to prepare all electrolytes.

3. Synthesis of $NaV_3O_8 \cdot 1.5H_2O$ (NVO) cathode material

The NVO powder was synthesized by a facile solution reaction method.[1] Typically, 2 g of commercial V_2O_5 powder was added into 30 mL of 2 M NaCl aqueous solution. After stirring for 4 days (96 h) at 30 °C, the suspension was thoroughly washed with deionized water for several times. Eventually, the black red product was obtained by freeze-drying.

4. Materials characterizations

The morphology of Zn plating/stripping on Cu substrate and cycled Zn foils were identified by scanning electron microscope (SEM, JSM-IT800, Japan). The operation voltage and current were set as 20 kV and 75 μA under the SHL mode with a UHD detector. The working distance (WD) was 8 mm. X-ray diffraction (XRD) spectra of electrodes were obtained by using a Bruker D8 diffractometer with a scanning range of 10° to 80°. Fourier transform infrared (FTIR) spectroscopy of Zn foil was conducted with Thermo Scientific Nicolet iS20 spectrophotometer. The solvation structure of electrolytes was identified by Raman spectroscopy (Raman, HORIBA Scientific LabRAM HR Evolution, 532 nm laser). The 3D optical images of Zn plating/stripping were collected by using an optical profilometer of Bruker Contour GT-K 3D.

5. Electrochemical measurements

All Zn||Zn symmetric cells, Zn||Ti and Zn||Cu asymmetric cells, and Zn||NVO full cells were fabricated using CR2025 coin-type cell in atmosphere, tested by the Neware BTS-5 test system. The NVO electrode was prepared by mixing NVO, KB, and PVDF with a mass ratio of 7:2:1 in 850 μL NMP and then casted onto Ti foil with a doctor blade. The electrode was dried at 80 °C for 12 h in vacuum oven. The anode and cathode were all cut into disks with a diameter of 16 mm, assembled with GF/D as separator. The mass loading of cathode used in coin cell-based full cell tests was about 1.5 mg cm^{-2}. The Zn||NVO pouch cell was consist of a Zn foil of 20 μm in thickness and a NVO cathode with each electrode area of 5×8 cm^2. The electrolyte addition was 1.5 mL. All cells were rested for 6 h prior to electrochemical tests. Cyclic voltammetry (CV), chronoamperometry (CA), linear polarization tests, linear sweep voltammetry (LSV) and electrochemical impedance spectroscopy (EIS) were performed on the CHI760E electrochemical workstation. The CV curves of Zn||Ti cells were carried out at a scan rate of 2 mV s^{-1} between –0.3 to 0.6 V. As for Zn||NVO full cells, the scan rate was 0.2 mV s^{-1} and the voltage range was between 0.5-1.5 V. The CA tests were conducted under certain overpotentials. Linear polarization tests were performed at a scan rate of 0.01 V s^{-1} in Zn||Zn symmetric cells. A three-electrode system was used to obtain LSV results, where Zn foil is the working electrode, Ti foil is the counter electrode, and Ag/AgCl electrode is the reference electrode. EIS spectra were conducted with a frequency range of 0.01-10^6 Hz.

The ionic conductivity (σ) of electrolyte was calculated by:

$$\sigma = \frac{L}{SR} \#(S1)$$

where L and S are the distance between two carbon-coated platinum electrodes and the area of testing electrode, R is the bulk resistance derived from the high-frequency intercept in EIS spectrum. Given that the σ and R of 3 M KCl standard solution at 25 °C are 86.22 mS cm^{-1} and 12.88 Ω, the σ of testing solution can be derived by Equation S1 with corresponding R.

The transfer number of Zn^{2+} ion (t) of electrolyte was calculated by:

$$t = \frac{I_{ss}(\Delta V - I_0 R_0)}{I_0(\Delta V - I_{ss} R_{ss})} \#(S2)$$

where ΔV is the applied overpotential (5 mV), I_{ss} and I_0 represent the steady-state current and initial current, R_{ss} and R_0 are the charge transfer resistances of steady-state and initial state.

6. Calculations details

In this study, first-principles calculations were performed using the Vienna Ab initio Simulation Package (VASP) package with the projector augmented wave (PAW) method.[2-4] The Perdew-Burke-Ernzerhof (PBE) exchange-correlation functional,[5] augmented with the D3 dispersion correction and Becke-Johnson damping function,[6] was employed to accurately describe adsorption interactions. The energy cutoff was set at 450 eV, and a Γ-centered k-point mesh of 2×2×1 grid was used for adsorption calculations. Convergence criteria for force and energy were established at 0.03 eV/Å and 10^{-5} eV, respectively. A vacuum layer of 15 Å was implemented, and simulations were conducted on an 8×8 supercell (256 Zn atoms) with a four-layer Zn (002) slab, where the bottom two layers were constrained to emulate bulk properties. The climbing image nudged elastic band (CI-NEB) method was then applied to explore the diffusion energy barrier for Zn adatom on the Zn surface, with a convergence criterion for energy set to 10^{-7} eV for high accuracy.[7] The diffusion pathway was divided into eight points except initial state and final state to comprehensively capture the diffusion process. Crystal structures were visualized using VESTA and VMD, and data post-processing was carried out using the VASPKIT code to extract pertinent information for analysis and interpretation.[8-10] The adsorption energy (E_{ad}) between Zn (002) slab and different adsorbate molecules (water and cordycepin) was defined as following equation:

$$E_{ad} = E_{Zn(002)+Molecules} - E_{Zn(002)} - E_{Molecules} \#(S3)$$

where $E_{Zn(002)+Molecules}$, $E_{Zn(002)}$ and $E_{Molecules}$ represent the total energies of the Zn (002) slab with adsorbed molecules, Zn (002) slab, and adsorbate molecules, respectively.

Results and Discussion

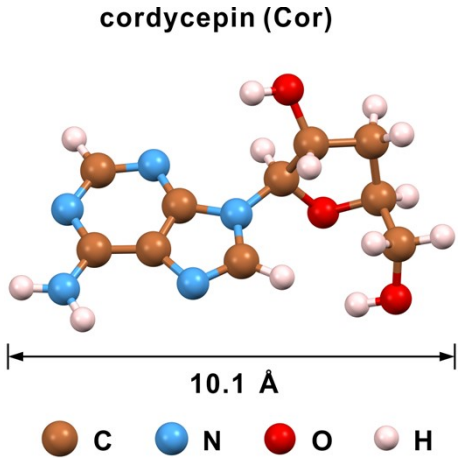

Fig. S1 The molecular structure of Cor.

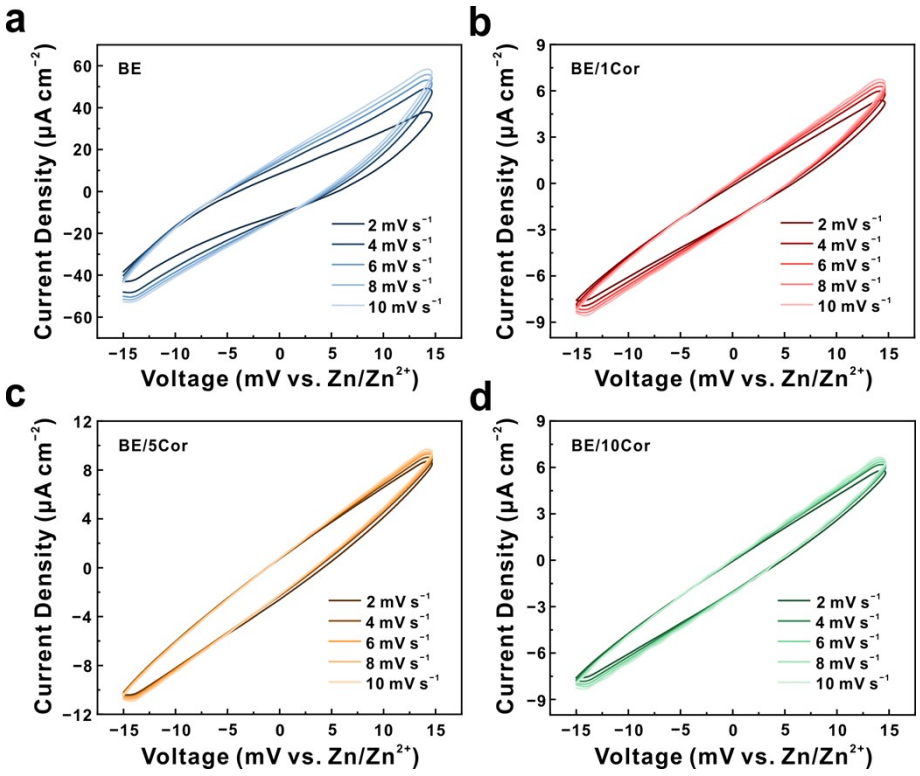

Fig. S2 CV curves of Zn||Zn symmetric cells with increasing scan rates from 2 to 10 mV s^{-1} in (a) BE; (b) BE/1Cor; (c) BE/5Cor; and (d) BE/10Cor electrolytes.

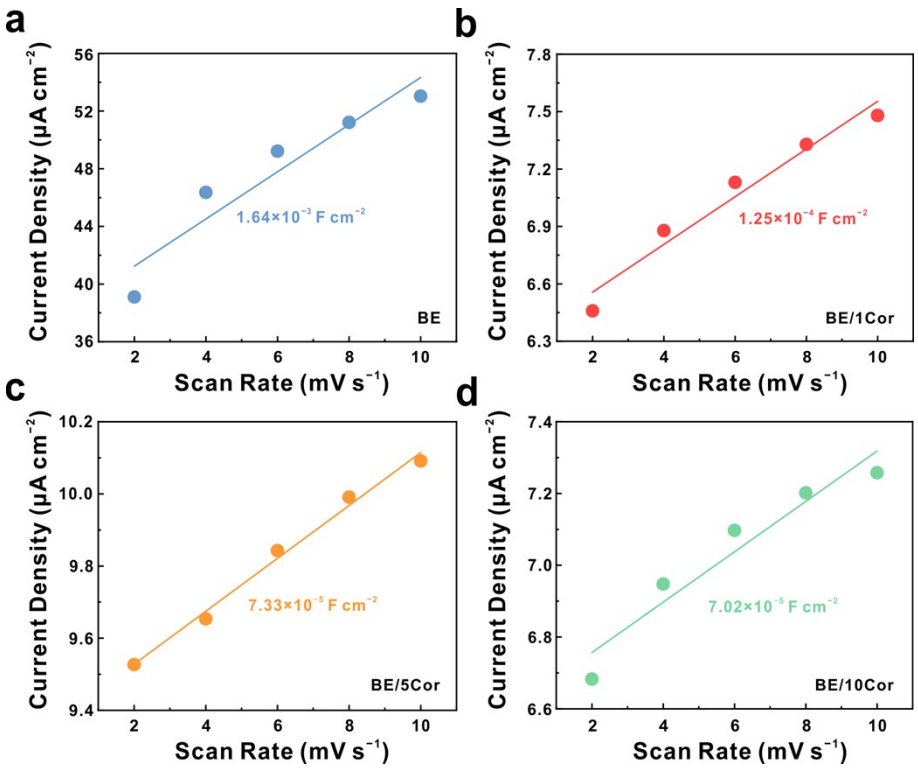

Fig. S3 The corresponding current density versus scan rate plots revealing the average differential capacitance of Zn anode in (a) BE; (b) BE/1Cor; (c) BE/5Cor; and (d) BE/10Cor electrolytes.

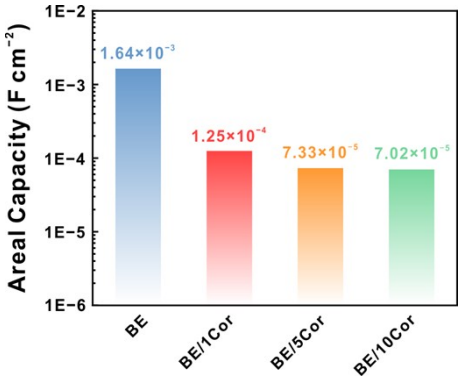

Fig. S4 Average differential capacitance for Zn anode with various concentrations of Cor.

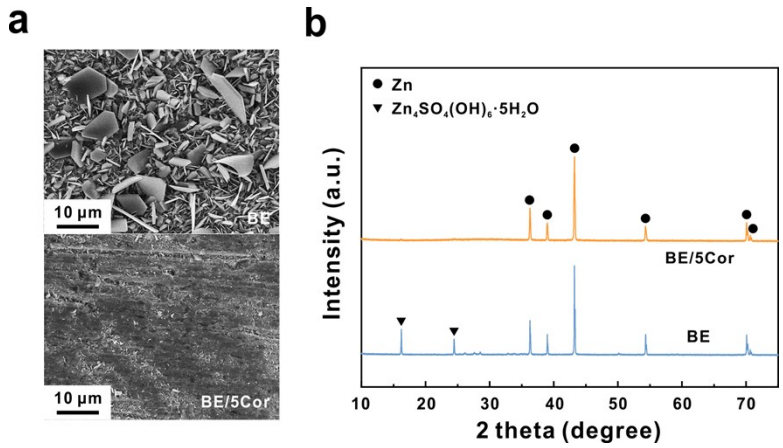

Fig. S5 (a) SEM images of Zn foils immersed in BE and BE/5Cor electrolytes for 7 days. (b) The corresponding XRD patterns.

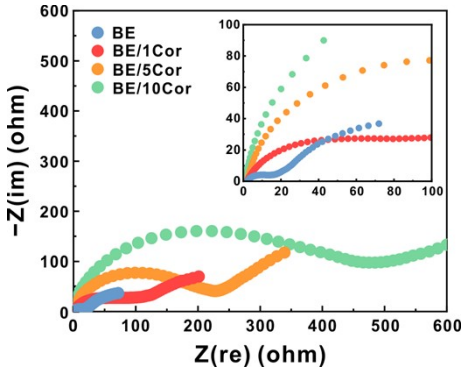

Fig. S6 EIS spectra of Zn||Zn symmetric cells assembled with polished Zn foils. Each side of the Zn foil is polished for three times with the sandpaper of 2000#.

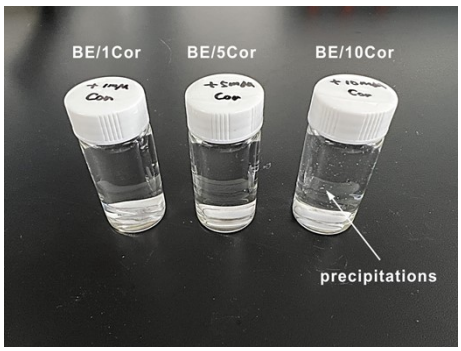

Fig. S7 The optical photo of different electrolytes. Obviously, the aqueous solution can maintain transparent when the concentration of Cor is low (1 and 5 mM), while with the presence of suspending precipitations at a high concentration (10 mM).

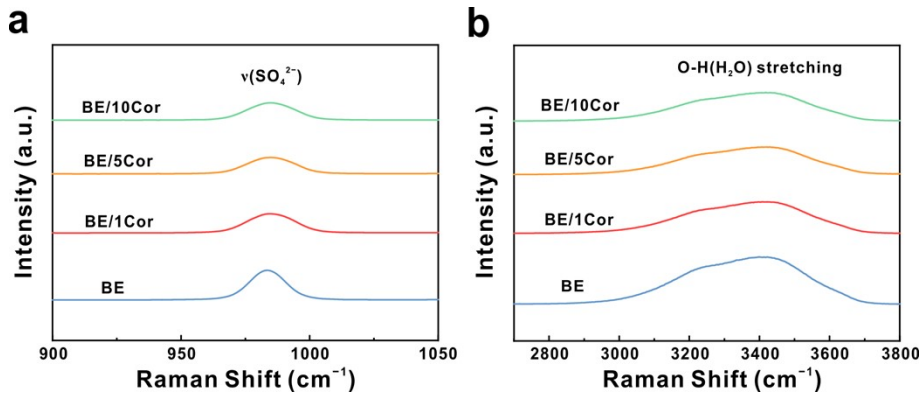

Fig. S8 Raman spectra of (a) the vibration of SO_4^{2-} and (b) the O-H stretching vibration of different electrolytes.

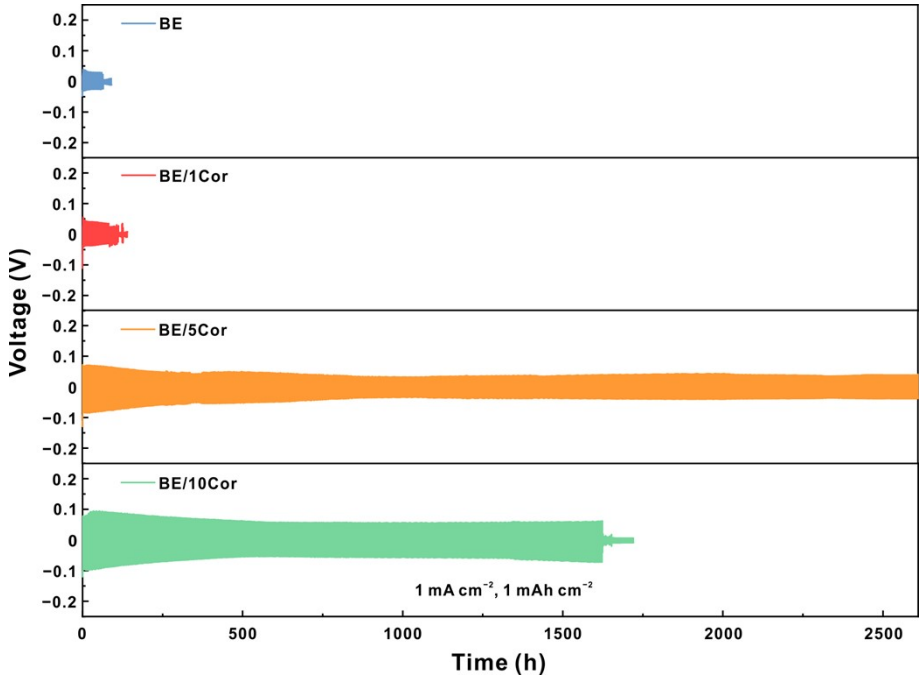

Fig. S9 Voltage profiles of Zn||Zn symmetric cells galvanostatically cycled at 1 mA cm^{-2} and 1 mAh cm^{-2}.

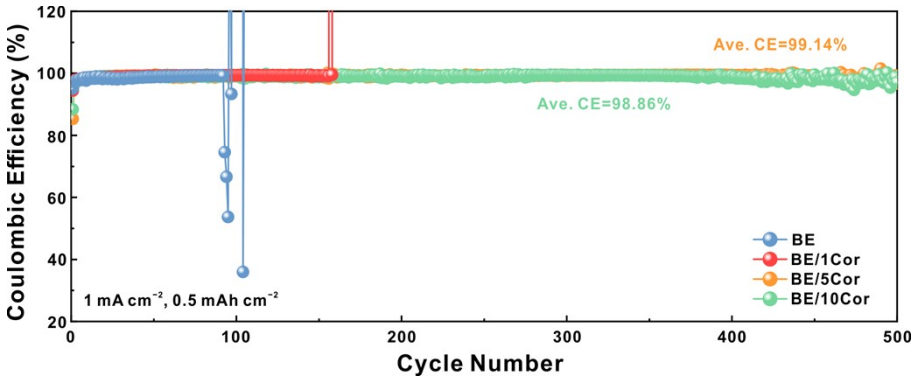

Fig. S10 CE comparisons of Zn||Cu asymmetric cells at 1 mA cm^{-2} and 0.5 mAh cm^{-2}.

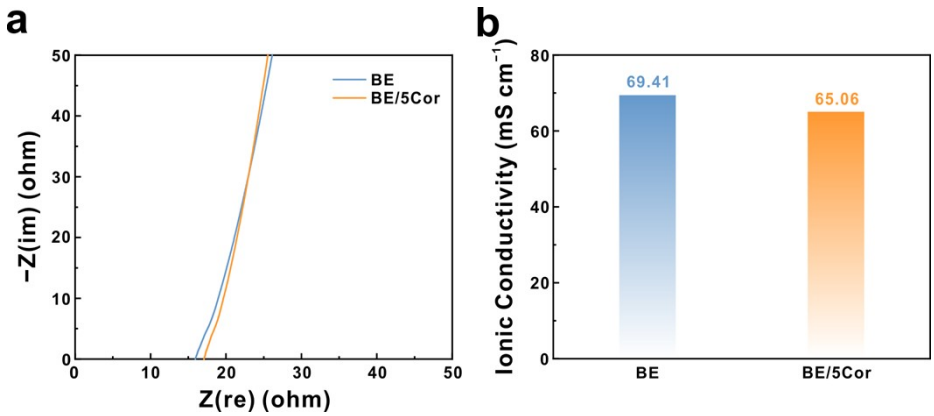

Fig. S11 (a) EIS spectra and (b) ionic conductivities of BE and BE/5Cor electrolytes.

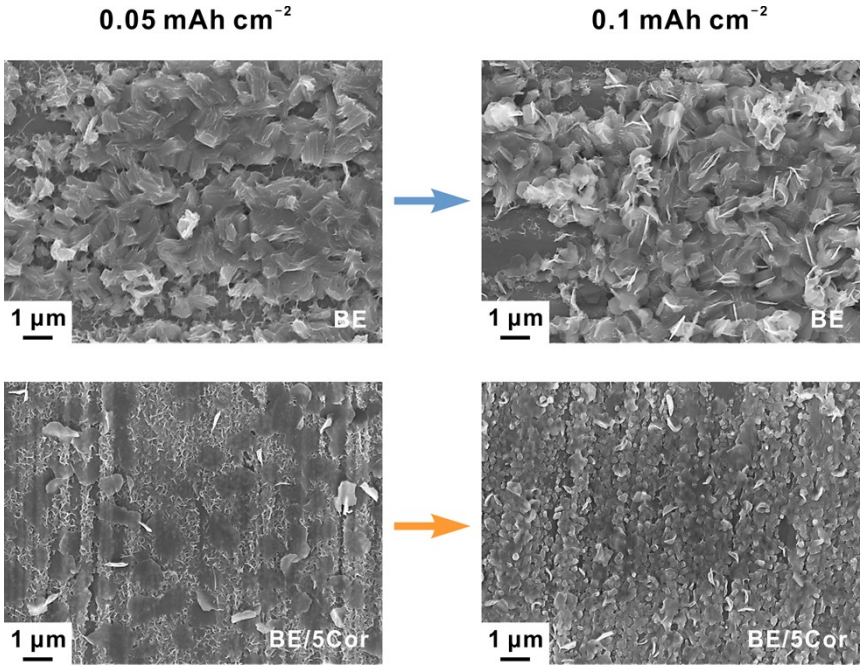

Fig. S12 SEM images of electrodeposited Zn with the areal capacities of 0.05 and 0.1 mAh cm^{-2} in BE and BE/5Cor electrolytes.

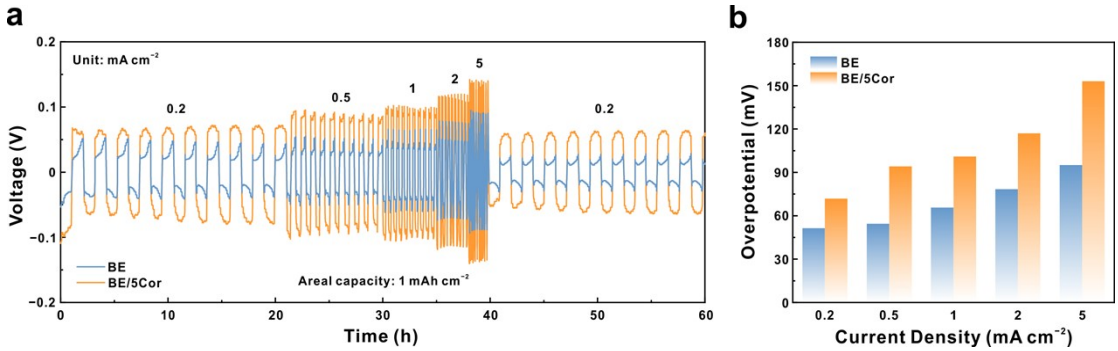

Fig. S13 (a) Rate performance of Zn||Zn symmetric cells with a fixed areal capacity of 1 mAh cm^{-2}. (b) The corresponding overpotentials under different current densities.

In addition to the enlarged voltage hysteresis, the shape of the charge-discharge curves in BE/5Cor also changed significantly compared with BE, which may manifest in two aspects: (1) the significant reduction of nucleation overpotential ($|\eta_n|$, the potential difference between the initial dip and the subsequent stable plateau region during electro-deposition); (2) the vanishment of charge/discharge plateaus. These changes are reasonable since the added Cor prominently alters the interfacial reaction processes. Specifically, as we confirmed in Fig. 2g, Cor could significantly amplify the surface overpotential ($|\eta_s|$), thus simultaneously reducing the nucleation energy barrier (based on the Equation 1-2), which corresponding to a much smaller $|\eta_n|$. On the other hand, the strong steric hinderance effect of Cor moderates the Zn/Zn^{2+} redox kinetics, inevitably exacerbating the concentration polarization of Zn^{2+} ions on the interface.[11,12] In this way, the charge accumulation would not be totally eliminated, which corresponding to the varying voltage.

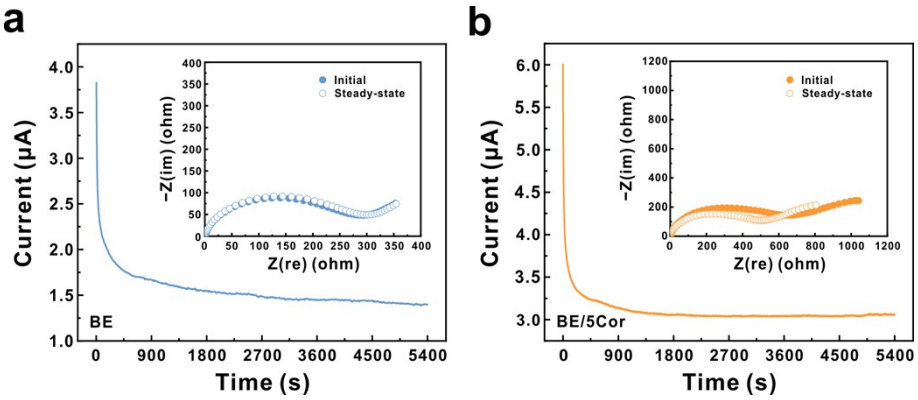

Fig. S14 CA curves of Zn||Zn symmetric cells at a constant overpotential of 5 mV for 5400 s in (a) BE and (b) BE/5Cor electrolytes. Insets show EIS spectra of cells at initial and after 5400 s.

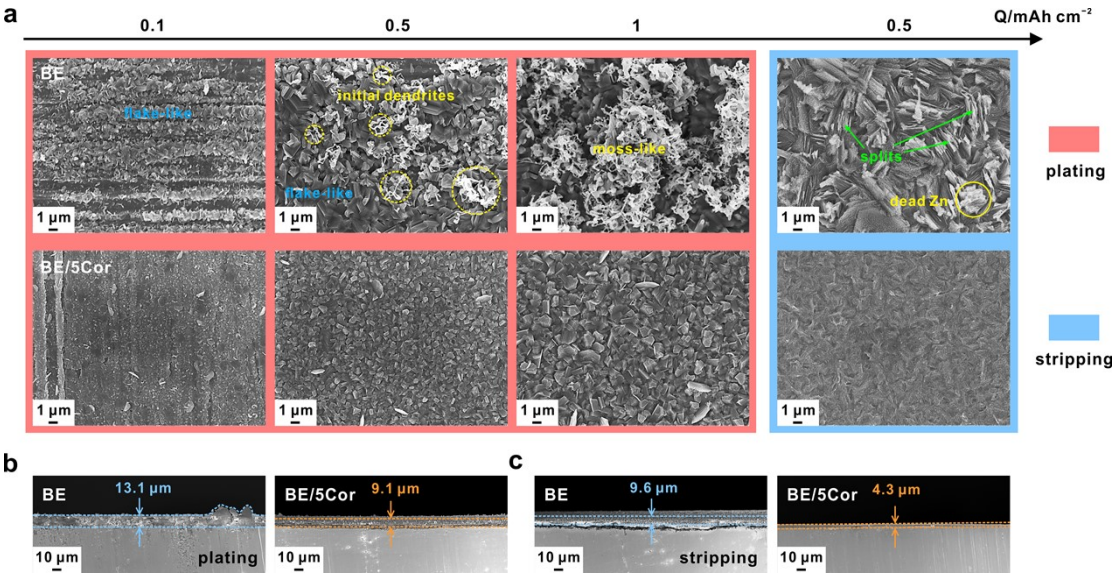

Fig. S15 (a) SEM images of plating 0.1, 0.5, and 1 mAh cm^{-2} of Zn on Cu substrate, respectively (inside the red rectangle), and stripping a half of the pre-deposited Zn with the capacity of 1 mAh cm^{-2} on Cu substrate (inside the blue rectangle). The applied current density is 5 mA cm^{-2}. Cross-sectional SEM images of (b) deposited Zn with the capacity of 1 mAh cm^{-2} on Cu substrate and (c) then stripping 0.5 mAh cm^{-2} of Zn at 5 mA cm^{-2}.

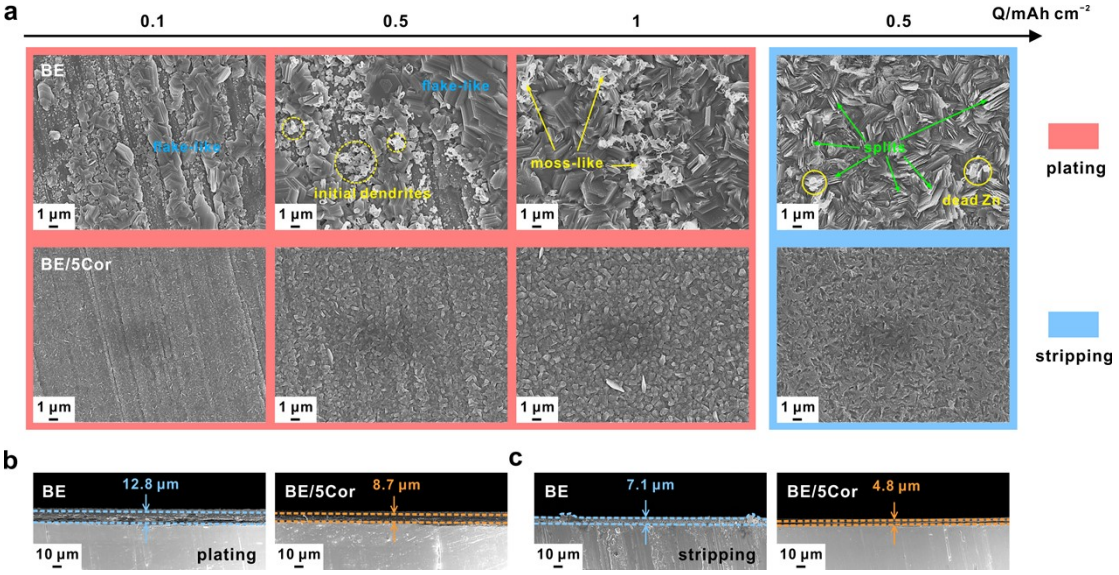

Fig. S16 (a) SEM images of plating 0.1, 0.5, and 1 mAh cm^{-2} of Zn on Cu substrate, respectively (inside the red rectangle), and stripping a half of the pre-deposited Zn with

the capacity of 1 mAh cm^{-2} on Cu substrate (inside the blue rectangle). The applied current density is 10 mA cm^{-2}. Cross-sectional SEM images of (b) deposited Zn with the capacity of 1 mAh cm^{-2} on Cu substrate and (c) then stripping 0.5 mAh cm^{-2} of Zn at 10 mA cm^{-2}.

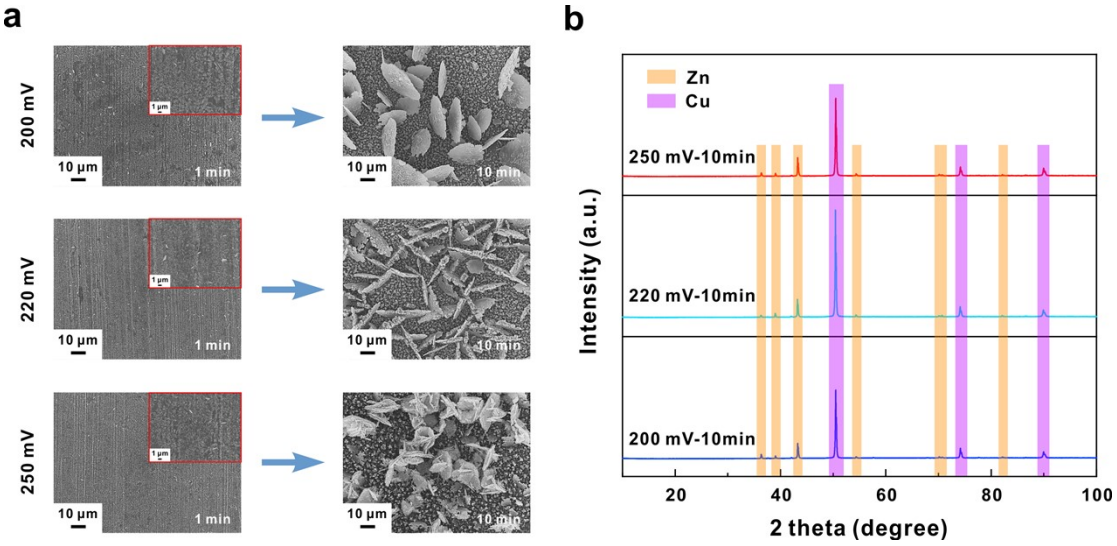

Fig. S17 (a) SEM images of deposited Zn on Cu substrate under the overpotentials of –200, –220, and –250 mV for 1 and 10 min in BE electrolyte. (b) The corresponding XRD patterns of deposited Zn for 10 min.

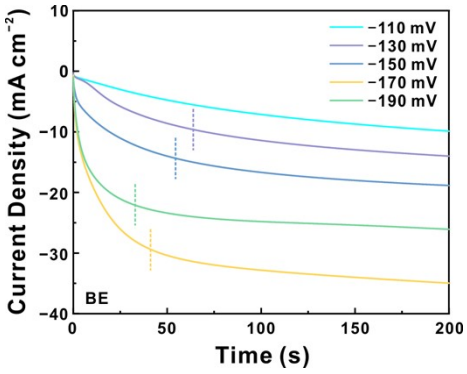

Fig. S18 CA curves of Zn||Zn symmetric cell under different external overpotentials with BE electrolyte.

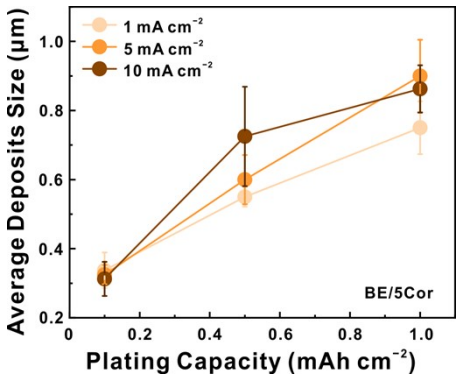

Fig. S19 The variation of average deposits size at different current densities with increasing plating capacities in BE/5Cor electrolyte.

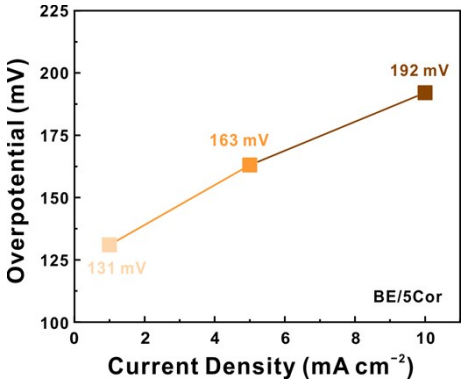

Fig. S20 The overpotential of Zn||Zn symmetric cell with respect to different current densities when cycled in BE/5Cor electrolyte.

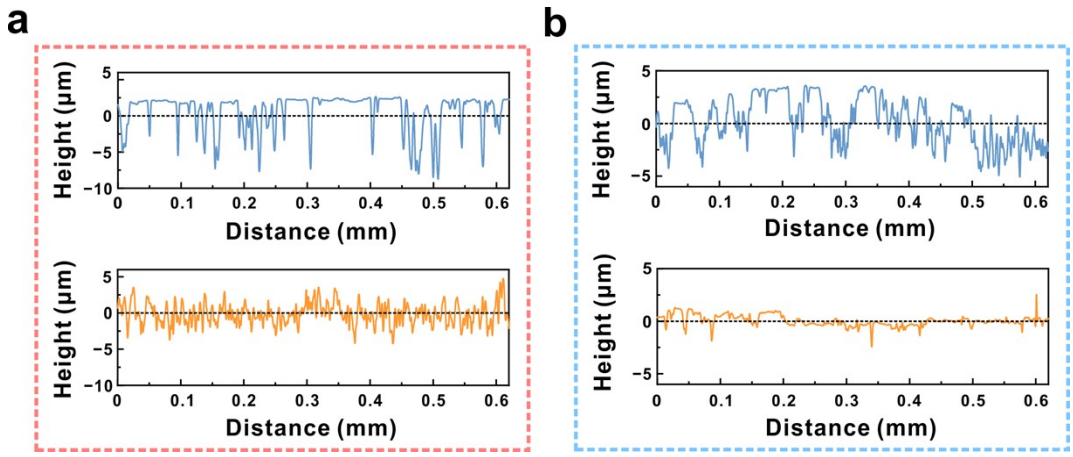

Fig. S21 The corresponding surface profiles extracted along the location marked with dotted white line in (a) Fig. 4b and (b) Fig. 4c.

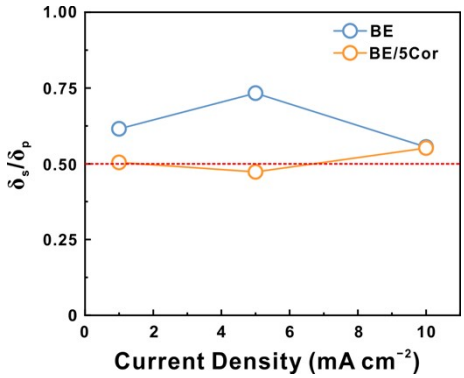

Fig. S22 The value of δ_s/δ_p in BE and BE/5Cor electrolytes with respect to different current densities.

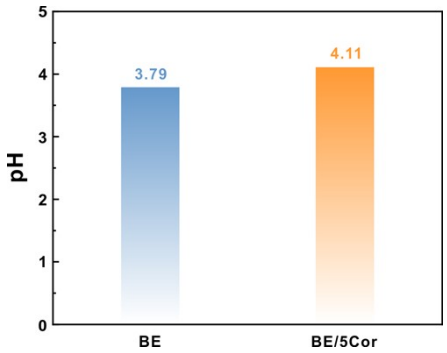

Fig. S23 The pH of BE and BE/5Cor electrolytes.

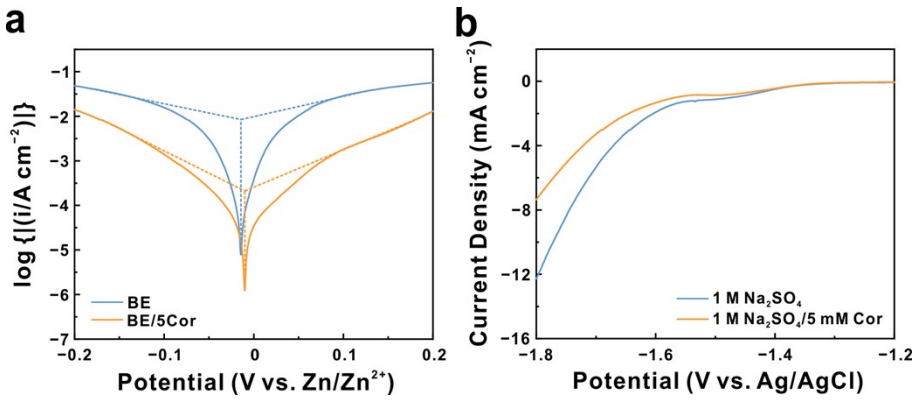

Fig. S24 (a) Linear polarization curves of Zn||Zn symmetric cells revealing the anti-corrosion property of Zn anode. (b) LSV curves of three-electrode beaker cells revealing the hydrogen evolution performance.

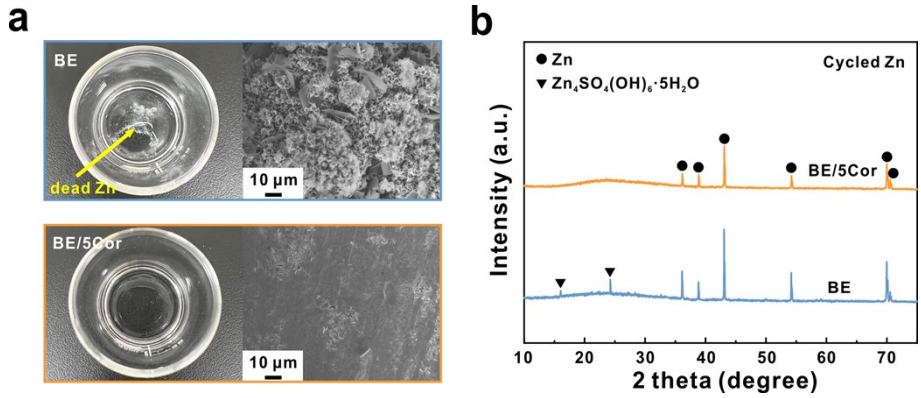

Fig. S25 (a) The optical photos of cycled electrolytes in beaker cells and SEM images of cycled Zn foils. (b) The corresponding XRD patterns of cycled Zn foils.

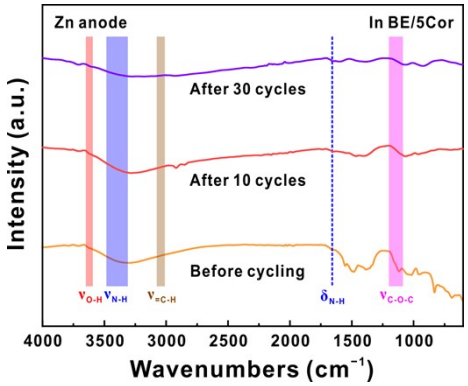

Fig. S26 FTIR spectra of Zn anode after different cycles in BE/5Cor electrolyte at 5 mA cm^{-2} and 5 mAh cm^{-2} compared with that before cycling.

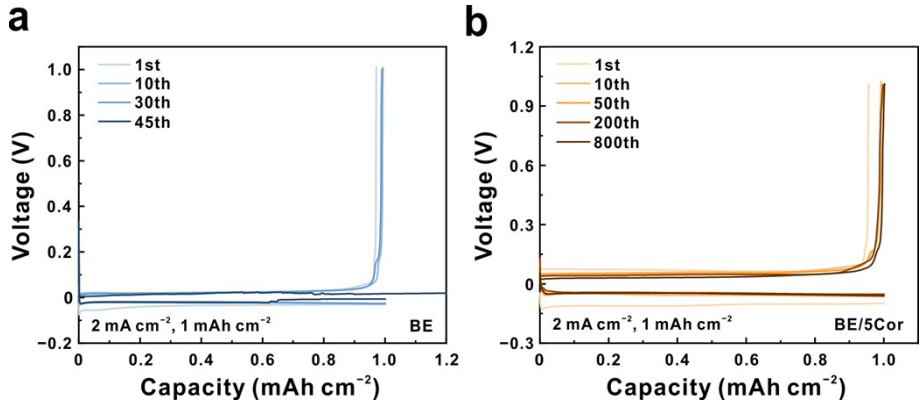

Fig. S27 The charge/discharge curves of Zn||Cu asymmetric cells at 2 mA cm^{-2} and 1 mAh cm^{-2} in (a) BE and (b) BE/5Cor electrolytes.

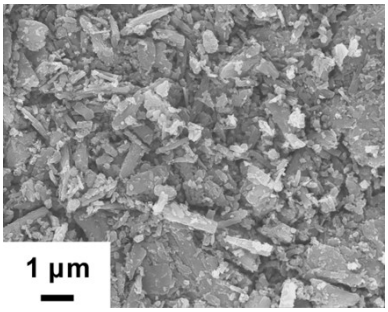

Fig. S28 SEM image of NVO cathode.

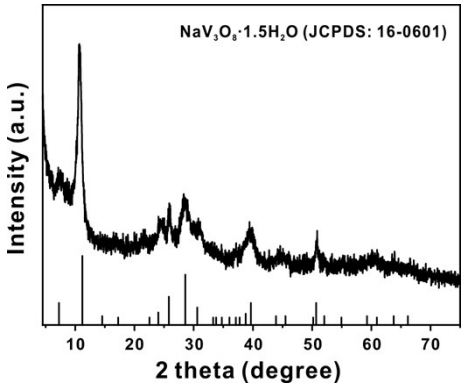

Fig. S29 XRD pattern of NVO cathode.

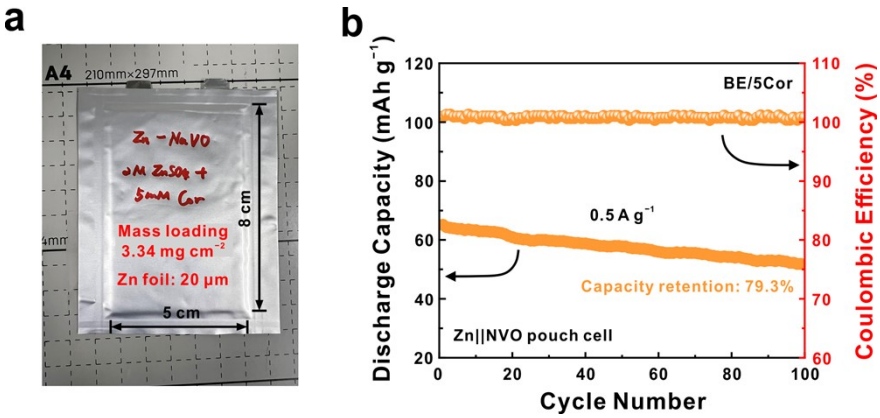

Fig. S30 (a) The optical photo of Zn||NVO pouch cell. (b) The corresponding long-term cycling performance at 0.5 A g^{-1}.

Table S1 Comparison of electrochemical performance in Zn||Zn symmetric cells with different additives.

Additive	Current density (mA cm^{-2})	Areal capacity (mAh cm^{-2})	Cycle lifespan (h)	CPC (Ah cm^{-2})	Ref.
5 mM Cor	**5**	**5**	**900**	**2.25**	**This work**
	10	**10**	**600**	**3**	
1% Py	0.5	0.5	3300	0.825	13
4 M Ch	1	1	2000	1	14
10 mM Glucose	1	1	2000	1	15
2 wt% TPPS	1	1	2300	1.15	16
5 mg mL^{-1} silk peptide	1	1	3000	1.5	17
0.05 mg mL^{-1} $Ti_3C_2T_x$	2	1	1100	1.1	18
10% TG	2	0.67	670	0.67	19
5 wt% MAAC	4	4	700	1.4	20
0.14 g L^{-1} Si-80HF	5	1	500	1.25	21
10 mM α-CD	10	1	160	0.8	22
0.1 M ImS	10	20	350	1.75	23
0.5 g L^{-1} TMBAC	10	5	475	2.375	24

40 mmol L^{-1} Na-L	10	5	500	2.5	25
0.01 M DLP	50	1	170	4.25	26
1.0 g L^{-1} BBI	10	10	1060	5.3	27

References

1. F. Wan, L. Zhang, X. Dai, X. Wang, Z. Niu and J. Chen, *Nat. Commun.*, 2018, **9**, 1656.
2. G. Kresse and J. Furthmüller, *Comp. Mater. Sci.*, 1996, **6**, 15-50.
3. G. Kresse and J. Furthmüller, *Phys. Rev. B*, 1996, **54**, 11169-11186.
4. P. E. Blöchl, *Phys. Rev. B*, 1994, **50**, 17953-17979.
5. J. P. Perdew, K. Burke and M. Ernzerhof, *Phys. Rev. Lett.*, 1996, **77**, 3865-3868.
6. S. Grimme, S. Ehrlich and L. Goerigk, *J. Comput. Chem.*, 2011, **32**, 1456-1465.
7. G. Henkelman, B. P. Uberuaga and H. Jónsson, *J. Chem. Phys.*, 2000, **113**, 9901-9904.
8. K. Momma and F. Izumi, *J. Appl. Crystallogr.*, 2011, **44**, 1272-1276.
9. W. Humphrey, A. Dalke and K. Schulten, *J. Mol. Graph.*, 1996, **14**, 33-38.
10. V. Wang, N. Xu, J.C. Liu, G. Tang and W. T. Geng, *Comput. Phys. Commun.*, 2021, **267**, 108033.
11. J. Wang, Q. Zhu, F. Li, J. Chen, H. Yuan, Y. Li, P. Hu, M. S. Kurbanov and H. Wang, *Chem. Eng. J.*, 2022, **433**, 134589.
12. Z. Tao, X. He, L. Yu, X. Ma, N. Ahmad and G. Zhang, *Small Methods*, 2024, 2400463.
13. J. Luo, L. Xu, Y. Zhou, T. Yan, Y. Shao, D. Yang, L. Zhang, Z. Xia, T. Wang, L. Zhang, T. Cheng and Y. Shao, *Angew. Chem., Int. Ed.*, 2023, **62**, e202302302.
14. X. Nie, L. Miao, W. Yuan, G. Ma, S. Di, Y. Wang, S. Shen and N. Zhang, *Adv. Funct. Mater.*, 2022, **32**, 2203905.
15. P. Sun, L. Ma, W. Zhou, M. Qiu, Z. Wang, D. Chao and W. Mai, *Angew. Chem., Int. Ed.*, 2021, **60**, 18247-18255.
16. X. Zhao, Y. Wang, C. Huang, Y. Gao, M. Huang, Y. Ding, X. Wang, Z. Si, D. Zhou and F. Kang, *Angew. Chem., Int. Ed.*, 2023, **62**, e202312193.
17. B. Wang, R. Zheng, W. Yang, X. Han, C. Hou, Q. Zhang, Y. Li, K. Li and H. Wang, *Adv. Funct. Mater.*, 2022, **32**, 2112693.
18. C. Sun, C. Wu, X. Gu, C. Wang and Q. Wang, *Nano-Micro Lett.*, 2021, **13**, 89.
19. Z. Liu, R. Wang, Q. Ma, J. Wan, S. Zhang, L. Zhang, H. Li, Q. Luo, J. Wu, T. Zhou, J. Mao, L. Zhang, C. Zhang and Z. Guo, *Adv. Funct. Mater.*, 2024, **34**, 2214538.
20. L. Zheng, H. Li, X. Wang, Z. Chen, C. Hu, K. Wang, G. Guo, S. Passerini and H. Zhang, *ACS Energy Lett.*, 2023, **8**, 2086-2096.
21. H. Wu, W. Yan, Y. Xing, L. Li, J. Liu, L. Li, P. Huang, C. Lai, C. Wang, W. Chen and S. Chou, *Adv. Funct. Mater.*, 2024, **34**, 2213882.

22. K. Zhao, G. Fan, J. Liu, F. Liu, J. Li, X. Zhou, Y. Ni, M. Yu, Y. M. Zhang, H. Su, Q. Liu and F. Cheng, *J. Am. Chem. Soc.*, 2022, **144**, 11129-11137.
23. Y. Lv, M. Zhao, Y. Du, Y. Kang, Y. Xiao and S. Chen, *Energy Environ. Sci.*, 2022, **15**, 4748-4760.
24. K. Guan, L. Tao, R. Yang, H. Zhang, N. Wang, H. Wan, J. Cui, J. Zhang, H. Wang and H. Wang, *Adv. Energy Mater.*, 2022, **12**, 2103557.
25. Z. Hu, F. Zhang, A. Zhou, X. Hu, Q. Yan, Y. Liu, F. Arshad, Z. Li, R. Chen, F. Wu and L. Li, *Nano-Micro Lett.*, 2023, **15**, 171.
26. Q. Zhu, G. Sun, S. Qiao, D. Wang, Z. Cui, W. Zhang and J. Liu, *Adv. Mater.*, 2024, **36**, 2308577.
27. Y. X. Song, J. Wang, X. B. Zhong, K. Wang, Y. H. Zhang, H. T. Liu, L. X. Zhang, J. F. Liang and R. Wen, *Energy Storage Mater.*, 2023, **58**, 85-93.